



CrossMark
 click for updates

Cite this: *RSC Adv.*, 2015, 5, 34398

Preparation and characterization of Ni/mZSM-5 zeolite with a hierarchical pore structure by using KIT-6 as silica template: an efficient bi-functional catalyst for the reduction of nitro aromatic compounds

Omid Mazaheri^a and Roozbeh Javad Kalbasi^{*b}

Ni/mZSM-5 and Ni/H-mZSM-5 were synthesized as hierarchical (micro/meso porous) ZSM-5 zeolites by an indirect template method for the first time. The resulting zeolite materials exhibited significantly enhanced diffusional properties in comparison to purely microporous zeolite materials. The structural and morphological characterization of the prepared catalysts was investigated using XRD, BET, atomic absorption spectroscopy, FT-IR, ²⁷Al-MAS NMR, SEM, TEM, XPS and DRS-UV techniques. These hierarchical zeolites were used as acid-metal bi-functional heterogeneous catalysts for hydride transfer in the reduction of nitro aromatic compounds. In these reactions, NaBH₄ was used as a reducing agent. Excellent yields at room temperature and very short reaction times in aqueous media conditions were obtained. Reusability experiments showed the excellent stability of Ni/mZSM-5 and Ni/H-mZSM-5 and the catalysts could be reused 7 times without much loss of activity in reduction of nitro aromatic compounds. Surprisingly, the acid form of Ni/H-mZSM-5 showed much higher activity than that of Ni/mZSM-5. High yield, short reaction time, green solvent (water), room temperature, no by-product, the easy reusability of catalysts and the low amounts of catalyst required are some of the advantages of these catalysts.

Received 6th February 2015
 Accepted 7th April 2015

DOI: 10.1039/c5ra02349a

www.rsc.org/advances

Introduction

In recent years, many new reagents have been developed for the reduction of aromatic nitro compounds into their corresponding aryl amines^{1,2} because many aryl amines exhibit biological activities, which have found numerous industrial applications, being intermediates for the synthesis of dyes, herbicides, pharmaceuticals, chelating agents, polymers, rubber materials, agricultural chemicals and surfactant textile auxiliaries.^{3–5} Also, they can be employed as a precursor and can be transformed into several other groups (amides, imines, *etc.*).^{6,7}

One of the conventional and interesting methods for the reduction of nitro aromatic compounds is Catalytic Transfer Hydrogenation (C.T.H).^{8,9} C.T.H represents a special variation of catalytic hydrogenation in which a catalyst and hydrogen gas are replaced with a catalyst and hydrogen donor such as hydrazine hydrate, NaBH₄, formic acid or propan-2-ol.¹⁰ In comparison to other methods, C.T.H has potential advantages including operational simplicity, no highly diffusible, no

flammable hydrogen gas is used and no special equipment are required.¹¹ In this regard, a lot of catalysts have been used in the reduction of nitro aromatic compounds among which heterogeneous catalysts compared to homogeneous ones have many advantages such as separation and recovery capabilities.^{12,13}

In recent years, various metal nanoparticles such as Pt, Pd, Au, Cu and Ni have been used as hydride transfer catalysts in the reduction of nitro aromatic compounds.^{14–20} However, in catalytic applications, a uniform dispersion of nanoparticles and an effective control of particle size are usually expected. However, nanoparticles frequently aggregate to yield bulk-like materials, which greatly reduce the catalytic activity and selectivity. Therefore, they must be embedded in matrices such as polymer or macromolecular organic ligands,^{21–23} or immobilized in the pores of heterogeneous supports like ordered mesoporous silica.²⁴ Additionally, porous materials such as alumina, silica and zeolites have many advantages as supports due to their high surface areas and their easy separation from reaction mixtures.

It has been proved that in the reduction of nitro compounds, acidic properties of supports can be helpful to promote the reaction.²⁵ Mesoporous silica (*e.g.* KIT-6) does not have acidic properties by itself; so it must be functionalized. On the other hand, zeolites are very versatile catalysts that can be tailored to

^aDepartment of Chemistry, Islamic Azad University, Shahreza Branch, 311-86145, Isfahan, Iran

^bFaculty of Chemistry, Kharazmi University, Tehran, Iran. E-mail: rkalbasi@gmail.com; Fax: +98 21 88820992; Tel: +98 21 88848949

achieve optimum performance in a wide range of catalytic reactions because of their regular porous structure with excellent stability and strong acidity.^{26,27} But the results indicated a poor adsorption capacity because of the diffusion limitation in the microporous network.²⁸ In recent years, hierarchical zeolites containing both microporosity and mesoporosity have been synthesized to exploit the shape selective properties of microporous zeolites while decreasing the diffusion and accessibility limitations of larger molecules in biomass upgrading.²⁹ In general, hierarchical zeolites can be obtained by template (use of solid templating, supramolecular templating, or indirect templating) and non-template (by demetallation) methods.³⁰ The post-synthetic demetallation is a non-template method, which often produces very random large pores in a wide pore size distribution although it has recently been developed to make uniform size of mesopores by desilication in the presence of cetyltrimethylammonium bromide (CTABr) surfactant.^{31,32} However, despite the fact that synthesis of zeolite using template method is more expensive, it will lead to more regular pores.³³ Therefore, most of the synthesis methods known today make use of templates in order to control the generation of mesopores. Christensen³⁰ has given an excellent and comprehensive summary of work in this field. According to the results, the incorporation of mesopores in the zeolite material can reduce pore blocking caused by large molecules adsorbed to the surface. Thus, it can decrease deposition on and deactivation of the adsorbent.^{34,35} In this regard, in recent years, extensive researches have been done on preparation and application of these types of zeolites in various reactions such as the isomeric reaction, alkylation, acylation, hydrocracking and pyrolysis.^{36–38}

Our present paper reports the synthesis and application of Ni nanoparticles supported on hierarchical mZSM-5 zeolite as a novel acid–metal bi-functional heterogeneous catalyst. This novel heterogeneous catalyst was used effectively for the reduction of nitro aromatic compounds in water medium and in the presence of low amount of NaBH₄ as a reducing agent. Also, the catalytic activity of hierarchical Ni/mZSM-5 zeolite was compared with its acidic form (Ni/H-mZSM-5) to investigate the effect of acidic properties on the activity of the catalyst in the reduction of nitro aromatic compounds.

Experimental

Instruments and characterization

The samples were analyzed using FT-IR spectroscopy (using a PerkinElmer 65 in KBr matrix in the range of 4000–400 cm⁻¹). The BET specific surface areas, BJH pore size distribution and MP-plot of the samples were determined by adsorption-desorption of nitrogen at liquid nitrogen temperature using a Series BEL SORP 18. The X-ray powder diffraction (XRD) of the catalyst was carried out on a Bruker D8 Advance X-ray diffractometer using nickel filtered Cu K α radiation at 40 kV and 20 mA. Moreover, X-ray photoelectron spectrum (XPS) was recorded on ESCA SSX-100 (Shimadzu) using a non-monochromatized Mg K α X-ray as the excitation source. Scanning Electron Microscope (SEM) studies were performed on Hitachi S4160 FESEM. Transmission Electron Microscope

(TEM) observations were performed on a Philips CM30 electron microscope at an accelerating voltage of 300.00 kV in order to obtain information on the size of Ni nanoparticles and the DRS UV-vis spectrophotometer were recorded with JASCO spectrometer, V-670 from 190 to 2700 nm. A solid-state ²⁷Al MAS-NMR spectrum was acquired at 11.7 T using a Bruker Avance 500 spectrometer and a 5 mm Doty MAS probe spun at ~10–12 kHz. The chemical shift was referenced to Al(H₂O)₆³⁺ solution. For the measurement of nickel, a PerkinElmer AAnalyst 300 atomic absorption spectrophotometer was used. The wave length, slit width and linear range for Ni were 232 nm, 0.2 nm and 2 ppm, respectively. Temperature-programmed desorption of NH₃ (NH₃-TPD) was carried out on FINESORB-3010 equipped with a thermal conductivity detector.

The products were characterized by ¹H NMR and ¹³C NMR spectra (Bruker DRX-500 Avance spectrometer at 500.13 and 125.47 MHz, respectively). Melting points were measured on an electrothermal 9100 apparatus. All the products were known compounds and they were characterized by FT-IR, ¹H NMR and ¹³C NMR. All melting points are compared satisfactorily with those reported in the literature. The GC analysis was carried out on a Shimadzu (QP 2010) series and a DB-5 MS capillary column, (30 m \times 0.25 mm i.d., 0.25 μ m). The initial temperature of the column was 75 $^{\circ}$ C held for 4 min. and was programmed to 235 $^{\circ}$ C at 4 $^{\circ}$ C min⁻¹, then it was held for 20 min. at 230 $^{\circ}$ C; the sample injection volume was 2 μ l in GC grade dichloromethane. Helium was used as carrier gas at a flow rate of 1.1 ml min⁻¹. The HPLC studies were performed on an Agilent 1100 HPLC-DAD (Agilent) and HIQ SIL C18 Column (4.6 mm \times 250 mm, 5 μ m) and UV-visible detector.

Catalysts synthesis

Preparation of KIT-6. To obtain the hierarchical zeolite, high quality ordered mesoporous KIT-6 silica was prepared firstly according to the reported procedure.³⁹ The large pore 3D (*Ia3d*) cubic mesostructure, designated as KIT-6, was prepared using Pluronic P123 (EO₂₀PO₇₀EO₂₀) template as a structure directing agent and tetraethylorthosilicate (TEOS) as the silica precursor. The detailed synthesis procedures are described as follows: 6 g (1.03 mmol) of P123 and 6 g of *n*-butanol (0.161 mol) were dissolved in 270 g (15 mol) of distilled water and 11.4 g (0.115 mol) of concentrated hydrochloric acid (37 wt% HCl). To this mixture, 12.9 g (0.061 mol) of TEOS was added. The mixture was stirred at 318 K for 24 h for the formation of mesostructure product. Subsequently, the reaction mixture was heated for 24 h at 370 K under static conditions for hydrothermal treatment. The solid product was then filtered, washed with deionized water and dried at 373 K. Finally, the samples were calcined at 823 K for 6 h to remove the organic template.

Preparation of hierarchical mZSM-5 zeolite. KIT-6 was used as an indirect template (silica source) for the synthesis of hierarchical zeolite. The hierarchical zeolite was prepared by the method described in recent literatures.⁴⁰ Briefly, a solution of sodium aluminate and tetrapropylammonium hydroxide (TPAOH, 40 wt%) was impregnated into 1 g of KIT-6 powder. The final molar ratio of the resulting synthesis gel was

$\text{Al}_2\text{O}_3 : 60\text{SiO}_2 : 4\text{Na}_2\text{O} : 4800\text{H}_2\text{O} : 18\text{TPAOH}$. The mixture was stirred for 12 h at room temperature. Then, the aged synthesis mixture was transferred into a Teflon-lined stainless steel autoclave followed by reaction at 448 K at different periods of 12, 24 and 48 h. The solid product was then filtered, washed with deionized water and dried in air at 393 K overnight. Finally, the samples were calcined at 823 K for 6 h to remove the TPAOH template, and the mZSM-5 product was obtained as a cream color powder.

Preparation of acid form of hierarchical zeolite (H-mZSM-5).

To investigate the effect of acidic sites of the zeolite on the catalytic activity, H-mZSM-5 was prepared and compared with mZSM-5. Therefore, 1 g of mZSM-5 was ion-exchanged with 100 mL aqueous solution of NH_4Cl (1 M) in the reflux condition for 48 h, washed with deionized water, dried at 383 K for 12 h and calcined at 823 K for 6 h to prepare hierarchical H-mZSM-5.

Preparation of Ni nanoparticles supported on hierarchical zeolites (Ni/mZSM-5 and Ni/H-mZSM-5). Ni/mZSM-5 and Ni/H-mZSM-5 were synthesized as follows: at first, 1 mL aqueous solution of $\text{NiCl}_2 \cdot 6\text{H}_2\text{O}$ (0.5 M) was added to the obtained mZSM-5 or H-mZSM-5 (0.1 g) together with 3 mL of H_2O . The mixture was heated for 5 h at 353 K. Then, the solution of NaBH_4 [0.057 g (1.5 mmol)] dissolved in 5 mL methanol was added to the mixture drop by drop in 20–30 min. After that, the solution was stirred for 3 h. Then, adding the same amount of NaBH_4 was repeated and again the mixture was stirred for 3 h. Afterwards, the solution was filtered and washed sequentially with deionized water and methanol to remove excess NaBH_4 and NiCl_2 , and was dried in room temperature to yield Ni/mZSM-5 and Ni/H-mZSM-5. The Ni content of the catalyst was estimated by decomposing. Known amount of the catalyst by perchloric acid, nitric acid, fluoric acid, hydrochloric acid, and the Ni content was estimated by atomic absorption spectrometer. The Ni content of Ni/mZSM-5 and Ni/H-mZSM-5 estimated by atomic absorption spectrometer was 2.1 mmol g^{-1} and 2.3 mmol g^{-1} , respectively.

General procedure for the reduction of nitro aromatic compounds. The reduction of nitro aromatic compounds in water solvent at room temperature was chosen as the standard reaction. In the typical experiment, a mixture of nitrobenzene (2 mmol), NaBH_4 (6 mmol) and Ni/mZSM-5 (0.04 g) or Ni/H-mZSM-5 (0.02 g) in water (3 mL) was placed in a 25 mL round bottom flask. The suspension was stirred at room temperature. Completion of the reaction was monitored by Thin Layer Chromatography (TLC), using *n*-hexane/ethylacetate (16 : 4) as an eluent. After the completion of the reaction, for the reaction work-up, the catalyst was removed from the reaction mixture by filtration, aniline was extracted from the aqueous medium by ether as an organic phase, and then the solvent was removed under reduced pressure. The products were obtained very pure just by extraction with ether in the majority of reactions. In a few cases, column chromatography was used to obtain the pure product. To ensure conversion and selectivity of the reactions, all reactions were followed using GC, which determined 100% conversion of nitrobenzene and its derivatives with selectivity of 100% towards aniline and its derivatives. However, isolated yields were preferred for report of the yields in tables instead of

GC yields. The product was identified with melting point, ^1H NMR, ^{13}C NMR and FT-IR spectroscopy techniques.

Results and discussion

Catalyst characterization

The low angle XRD pattern of KIT-6 is depicted in Fig. 1a. The XRD pattern of KIT-6 shows one intense peak at 2θ about 0.94° and two weak peaks at 2θ about 1.50° and 1.7° , which can be indexed as (211), (220) and (320) reflections associated with three-dimensional cubic symmetry ($Ia\bar{3}d$).^{39,41}

A time trial growth study was conducted for insight into the growth of the hierarchical mZSM-5. Crystalline characteristic of the products with reaction duration periods of 12, 24 and 48 h were analyzed using XRD (Fig. 1). As can be seen, with an increase in the crystallization time, the peak intensity of the KIT-6 was decreased (Fig. 1a), which is related to the partial transformation of zeolite precursor materials onto the mesopores of KIT-6 (indirect templating method). In addition, with an increase in the crystallization time, the peak intensity of ZSM-5 in the area of $2\theta = 7.9^\circ, 8.8^\circ, 23.3^\circ, 23.7^\circ$ and 24° is increased indicating an increase in the zeolite crystallinity.⁴²

The XRD pattern of the sample that has been crystallized for 12 h showed the amorphous pattern in $2\theta = 15\text{--}35^\circ$, and no clear peak was observed for the zeolite (Fig. 1b). On the other hand, the ordered mesoporous structure of KIT-6 still remains (Fig. 1a). After 24 h of crystallization time, some characteristic peaks can be seen in the $2\theta = 15\text{--}35^\circ$, which are related to the formation of crystalline structure of the zeolites (Fig. 1b). At the same time, the peak intensity and sharpness of the characteristic peak of KIT-6 ($2\theta = 0.94^\circ$) are reduced, indicating that symmetrical structure of KIT-6 is reduced to some extent during crystallization of zeolite in the pores of KIT-6 (Fig. 1a). Finally, after 48 h of crystallization, some intense and sharp peaks in $2\theta = 15\text{--}35^\circ$ can be observed, and the symmetrical structure of KIT-6 has completely disappeared, which proves the successful formation of hierarchical mZSM-5 zeolites (in order to prove the formation of mZSM-5 structure, the XRD pattern of all samples was compared with ZSM-5 as a blank sample prepared by traditional method⁴²) (Fig. 1b). Thus, 48 hour hydrothermal condition was considered as an optimized time.

In Ni/mZSM-5, nickel peak cannot be seen in XRD due to the homogeneity of Ni particles in the Ni/mZSM-5, and it just shows an amorphous pattern at 2θ values of about 44° (Fig. 2, inside). In order to prove the existence of Ni nanoparticles in the hierarchical zeolite, Ni/mZSM-5 catalyst was exposed to temperature (400°C). On heating, amorphous Ni changed to crystalline, and appeared as a peak.^{12,14} The XRD patterns of Ni/mZSM-5 sample at 400°C can be seen in Fig. 2. After calcination at 400°C , XRD pattern of residue shows a broad peak with low intensity (about 44°), which can be attributed to the small size of nickel nanoparticles (Smaller than 10 nm) (Fig. 2, inside).¹² However, the peak at $2\theta = 44.29^\circ$ corresponds to the plane (111) of fcc nickel.¹⁴ Nevertheless, as can be seen, after the deposition of nickel nanoparticles on hierarchical zeolites, zeolite structure has not changed, representing a successful synthesis of the catalyst (Fig. 2). The XRD patterns of H-mZSM-5 and Ni/H-

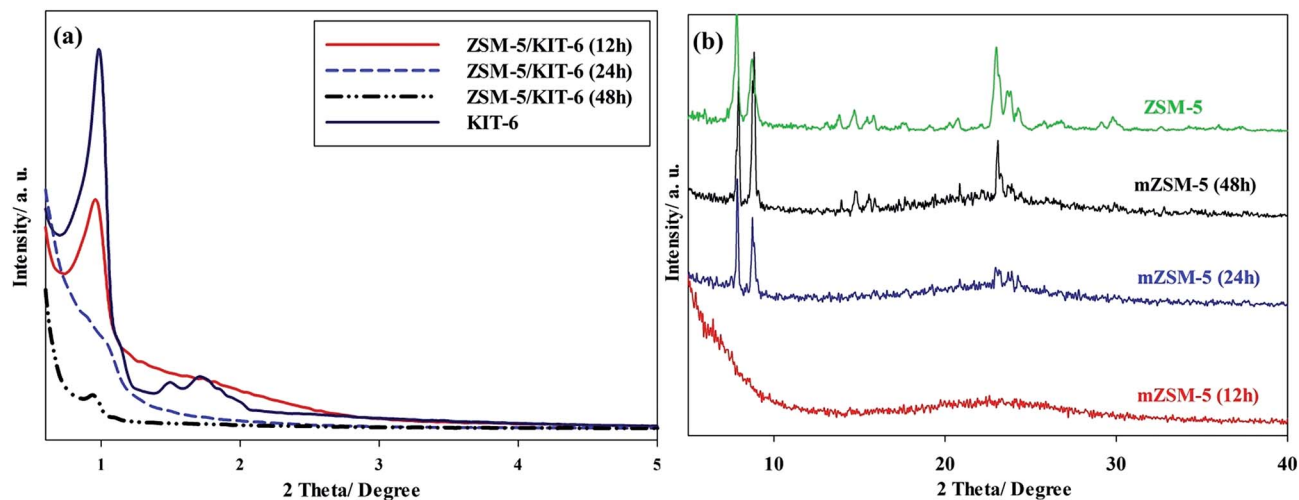


Fig. 1 (a) Low angle XRD patterns of mesoporous silica KIT-6 and mZSM-5 at different reaction periods: after 12 h, 24 h and 48 h crystallization, (b) wide angle XRD pattern of mZSM-5 at different reaction periods: after 12 h, 24 h and 48 h crystallization and conversional mZSM-5.

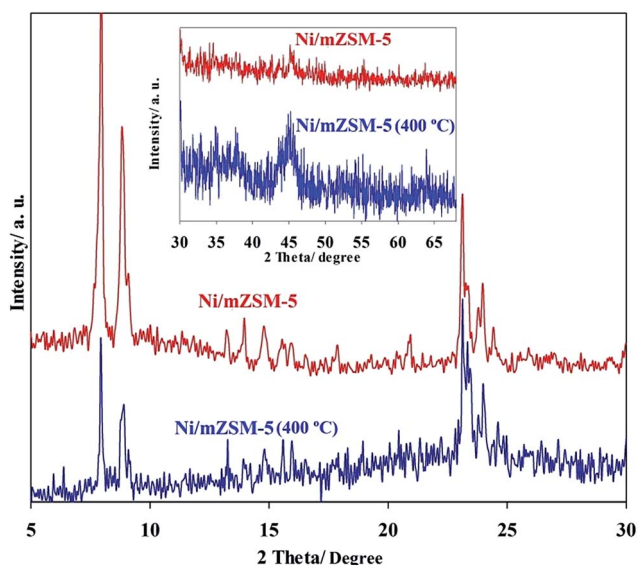


Fig. 2 XRD patterns of amorphous Ni/mZSM-5 and Ni/mZSM-5 burned in 400 °C for 4 h ($2\theta = 5-30$). Inside: amorphous Ni/mZSM-5 and Ni/mZSM-5 burned in 400 °C for 4 h ($2\theta = 30-65$).

mZSM-5 are depicted in Fig. 3. The results show that the crystalline structure of hierarchical zeolite is retained after preparation of acidic form of hierarchical zeolite (H-mZSM-5). In addition, the XRD pattern of Ni/H-mZSM-5 (heated on 400 °C) is the same as Ni/mZSM-5.

The BET specific surface areas, the pore volumes and the pore sizes of KIT-6, mZSM-5, Ni/mZSM-5, H-mZSM-5 and Ni/H-mZSM-5 samples were calculated using BET, BJH, MP-Plot and *t*-Plot methods (Table 1). The N₂ sorption isotherms for these samples are shown in Fig. 4 and 5. In addition, the corresponding pore size distribution curves (meso and micro pores) are plotted in Fig. 4–6. As shown, all samples depict isotherms similar to isotherms of type IV, which are the typical

characteristics of mesoporous materials (Fig. 4 and 5), according to the IUPAC nomenclature.⁴³

It is seen that KIT-6 has a high BET surface area ($988 \text{ m}^2 \text{ g}^{-1}$), a large pore volume ($1.35 \text{ cm}^3 \text{ g}^{-1}$) and pore size (8.06 nm), which indicates its applicability as a suitable supply for the growth of mZSM-5 zeolite (Table 1). It is clear that mZSM-5 exhibits a smaller specific surface area in comparison to those of pure KIT-6 and also the shape of the isotherm has been changed (Table 1 and Fig. 4).^{38,40} However, its isotherm is still similar to that of type IV, which is the typical characteristic of a mesoporous material. These results may be attributed to the formation of a new hierarchical zeolitic structure (mZSM-5) with a reasonable surface area and porosity. In addition, the co-presence of micropores is suggested by the N₂

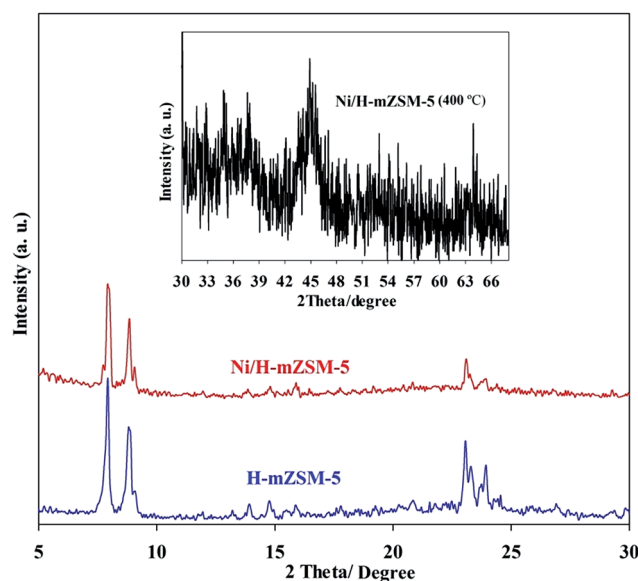


Fig. 3 XRD patterns of H-mZSM-5 and Ni/H-mZSM-5 ($2\theta = 5-30$) and inside: Ni/H-mZSM-5 burned in 400 °C for 4 h ($2\theta = 30-66$).

Table 1 Physicochemical properties of KIT-6, mZSM-5, H-mZSM-5, Ni/mZSM-5 and Ni/H-mZSM-5 samples obtained from N₂ adsorption

Sample	S_{mesopore}^a (m ² g ⁻¹)	V_{mesopore}^a (cm ³ g ⁻¹)	D_{mesopore}^b (nm)	$S_{\text{micropore}}^c$ (m ² g ⁻¹)	$S_{\text{micropore}}^d$ (m ² g ⁻¹)	$V_{\text{micropore}}^c$ (cm ³ g ⁻¹)	$D_{\text{micropore}}^c$ (nm)	IR crystallinity ^e (%)
KIT-6	988	1.35	8.06	—	—	—	—	—
mZSM-5	188	0.25	4.20	272	195	0.12	0.7	98
H-mZSM-5	223	0.26	4.60	269	225	0.10	0.7	99
Ni/mZSM-5	107	0.24	3.28	156	—	0.09	0.6	87
Ni/H-mZSM-5	60	0.23	2.4	85	—	0.08	0.8	91

^a Calculated by BET method. ^b Mean pore diameter determined by using BJH method from the adsorption branch of the isotherm curves. ^c Calculated by MP-Plot method. ^d The micropore surface area was estimated by the *t*-plot analysis using the adsorption branch of the isotherm curves. ^e IR crystallinity defined as $(I_{550}/I_{450})/0.72 \times 100\%$ (ref. 50) with I_{550} and I_{450} the intensities of the bands at 550 and 450 cm⁻¹, respectively.

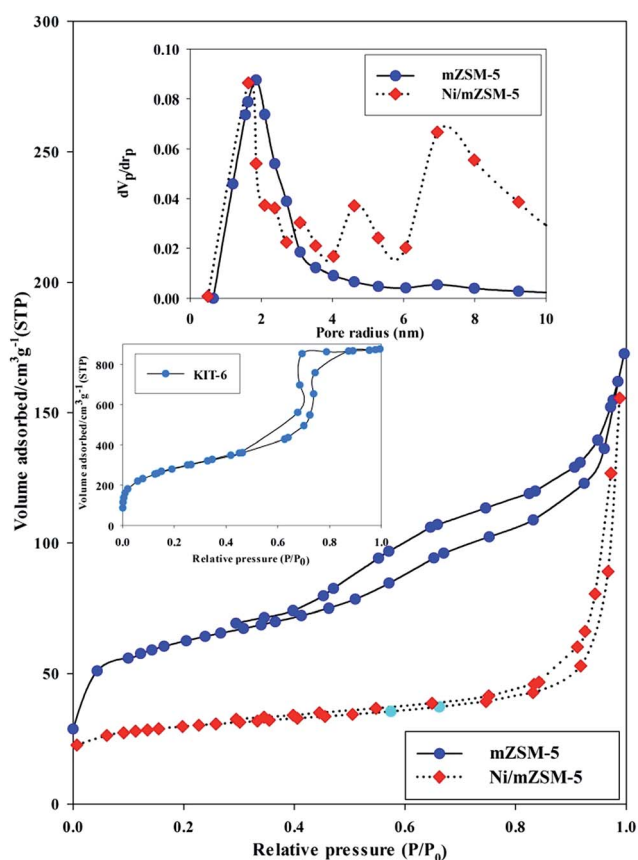


Fig. 4 N₂ adsorption–desorption isotherms of KIT-6, mZSM-5 and Ni/mZSM-5. Inside: pore size distributions of mZSM-5 and Ni/mZSM-5 obtained by BJH method.

adsorption isotherm using MP-Plot and *t*-Plot methods (Table 1). According to the results, mZSM-5 shows both microporous and mesoporous structures. Also, acidic form of mZSM-5 (H-mZSM-5) shows the same characteristics as mZSM-5, which means that the structure of mZSM-5 is well retained after acidification using ammonium cation. However, the surface area of H-mZSM-5 has increased in comparison to mZSM-5, which can be related to hydrothermal conditions in boiling water when ammonium cation is exchanged with sodium ion.⁴⁴

The specific surface area, pore volume and pore diameter (calculated by BJH) of Ni/mZSM-5 and Ni/H-mZSM-5 are lower than those of mZSM-5 and H-mZSM-5 (Table 1), which is due to the distribution of nickel nanoparticles on the outer surface and their incorporation inside the pores of the hierarchical zeolites. As can be seen from Table 1, the BET surface area and size of mesopores of Ni/mZSM-5 are larger than those of Ni/H-mZSM-5, while H-mZSM-5 has a higher surface area and larger mesopore size than mZSM-5. It can be related to the Ni contents of Ni/H-mZSM-5, which is about 9.5% higher than that of Ni/mZSM-5 (data are presented in Table 2).

Pore size distributions (using BJH method) of the synthesized materials are shown in Fig. 4 and 5 (inside). As shown, the samples of mZSM-5 and H-mZSM-5 have a narrow pore size

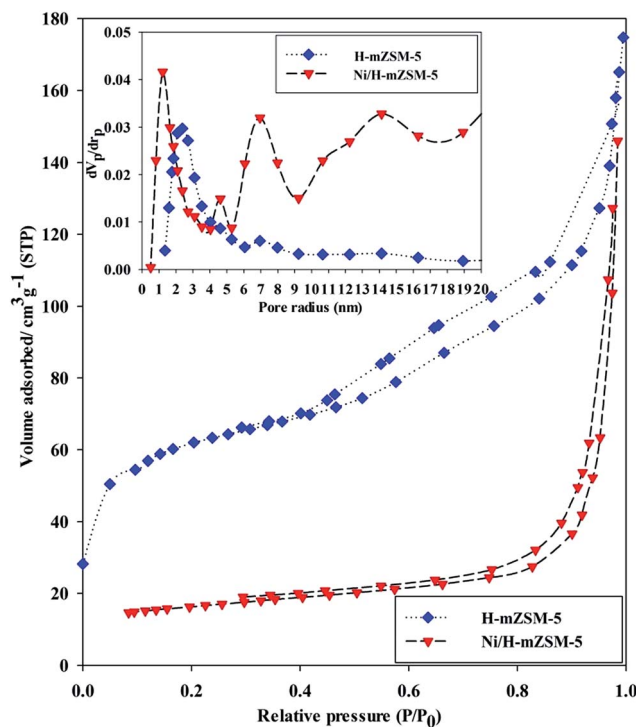


Fig. 5 N₂ adsorption–desorption isotherms of H-mZSM-5 and Ni/H-mZSM-5. Inside: pore size distributions of H-mZSM-5 and Ni/H-mZSM-5 obtained by BJH method.

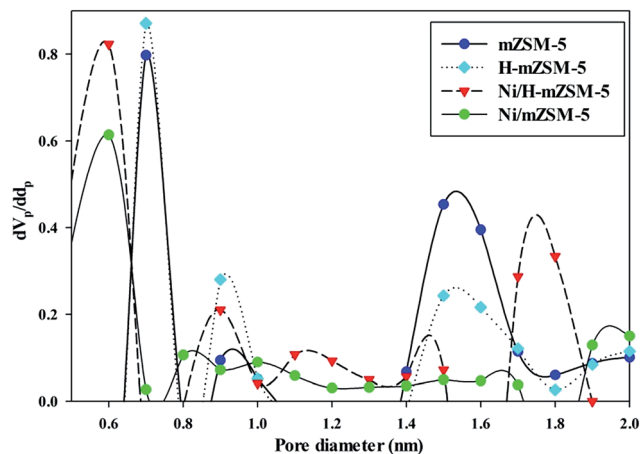


Fig. 6 Pore size distributions of mZSM-5, Ni/mZSM-5, H-mZSM-5 and Ni/H-mZSM-5 obtained by MP-Plot method.

distribution with a pore diameter of about ~ 4 nm indicating the presence of a mesoporous structure in these zeolites. After the incorporation of nickel nanoparticles, the pore size distribution is changed, which indicates the distribution of nickel nanoparticles on the surface of zeolites (Fig. 4 and 5). It is wise to mention that the pore size distribution of mZSM-5 is narrower than H-mZSM-5, so it can be expected that a higher number of nickel nanoparticles can be placed in the pores of the H-mZSM-5 (The Ni contents of the catalysts are presented in Table 2) and the pore diameter and surface area of Ni/H-mZSM-5 will be reduced more than those of Ni/mZSM-5 (Table 1).

Furthermore, *t*-Plot and MP-Plot methods confirm the existence of microporosity within the mZSM-5 and H-mZSM-5 structures (Table 1 and Fig. 6). After the incorporation of nickel nanoparticles, these microporous structures are still observable (Fig. 6).

Finally, according to the results, Ni/mZSM-5 and Ni/H-mZSM-5 still show a hierarchical structure with a reasonable surface area, pore volume and pore diameter, which make it suitable to act as catalyst.

Also, according to the TPD results, the numbers of acid sites were 0.96 mmol g^{-1} for H-mZSM-5 and 0.92 mmol g^{-1} for Ni/H-mZSM-5 (Table 1), respectively; which indicates that the acidic nature of the catalyst is retained. Therefore, despite the deposit of nickel nanoparticles on H-mZSM-5, acidic properties of Ni/H-mZSM-5 are still maintained.

^{27}Al -MAS NMR spectra of the central transitions for mZSM-5 and Ni/mZSM-5 are shown in Fig. 7. The spectrum exhibits a dominant resonance with a center of gravity at around 54 ppm, which originates from tetrahedral coordinated Al atoms in the framework.^{45,46} According to the results, the chemical shift of Al atoms is not changed after the incorporation of Ni nanoparticles in the pores of mZSM-5. Furthermore, the ^{27}Al -MAS NMR result clearly indicates the high stability of mZSM-5 and Ni/mZSM-5, as they may stand the calcination at 823 K treatment in spite of the presence of large pores in these zeolites.

The FT-IR spectra of pure KIT-6, Ni/KIT-6, ZSM-5, Ni/ZSM-5, mZSM-5 and Ni/mZSM-5 are shown in Fig. 8 (the FT-IR spectra

of H-mZSM-5 and Ni/H-mZSM-5 are not shown here since they are almost the same as the mZSM-5 and Ni/mZSM-5). A broad band at around 3440 cm^{-1} is observed in all samples. It is mainly caused by the O–H stretching vibration of the adsorbed water molecules and hydroxyl groups of silica surface. The band at about 1630 cm^{-1} is attributed to adsorbed water, which is basically similar to related reports.^{47,48} Absorption bands at around 1220 cm^{-1} (external asymmetric stretch), $1150\text{--}1050 \text{ cm}^{-1}$ (internal asymmetric stretch), $\sim 800 \text{ cm}^{-1}$ (symmetric stretch) and 450 cm^{-1} (T–O bend) are typical of highly siliceous materials. In the FT-IR spectrum of ZSM-5, mZSM-5 and Ni/mZSM-5 (Fig. 8), the new band at around 550 cm^{-1} corresponds to the double five rings of the characteristic structure of MFI-type zeolites.⁴⁰ Moreover, in the FT-IR spectrum of ZSM-5 and mZSM-5 (Fig. 8), the Si–OH–Al groups ($\sim 3650 \text{ cm}^{-1}$) are shown to be acidic (more specifically, they are Bronsted acid sites) and in agreement with previous reports.^{46,49} Both the XRD and the FT-IR spectra can indicate that MFI-type zeolite (mZSM-5) has been successfully synthesized.

Moreover, the ratio of the intensities of 550 and 450 cm^{-1} bands were used to calculate the (IR) crystallinity of the prepared samples. The results were also collected in Table 1. High IR crystallinity points to a high degree of ordering of the aluminosilicate phase in a manner similar to that in ZSM-5 zeolite.⁵⁰

The morphologies of the mZSM-5 and Ni/mZSM-5 are shown in Fig. 9. The synthesized mZSM-5 is small cubic regular particles with a crystalline form structure and a size about $5 \mu\text{m}$ (Fig. 9a–d). Actually, the morphology of mZSM-5 is cubic thanks to the cubic structure of KIT-6 as template (Fig. 9a–d).

As can be seen, there is a difference in particle surface morphology between the mZSM-5 host and Ni/mZSM-5 (Fig. 9e and f) indicating that some of the Ni nanoparticles are distributed on the outer surface of the zeolite. It is necessary to mention that some of the Ni nanoparticles are incorporated inside the zeolite mesoporous structure, which is not observable in the SEM images (these particles can be seen in the TEM

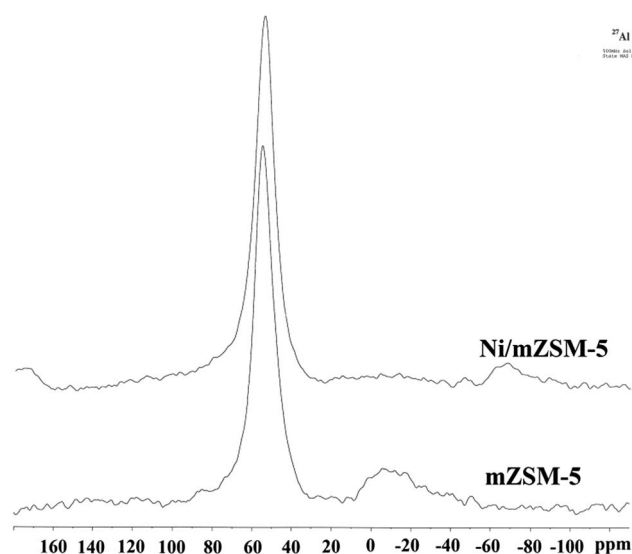


Fig. 7 ^{27}Al -MAS NMR spectra of mZSM-5 and Ni/mZSM-5.

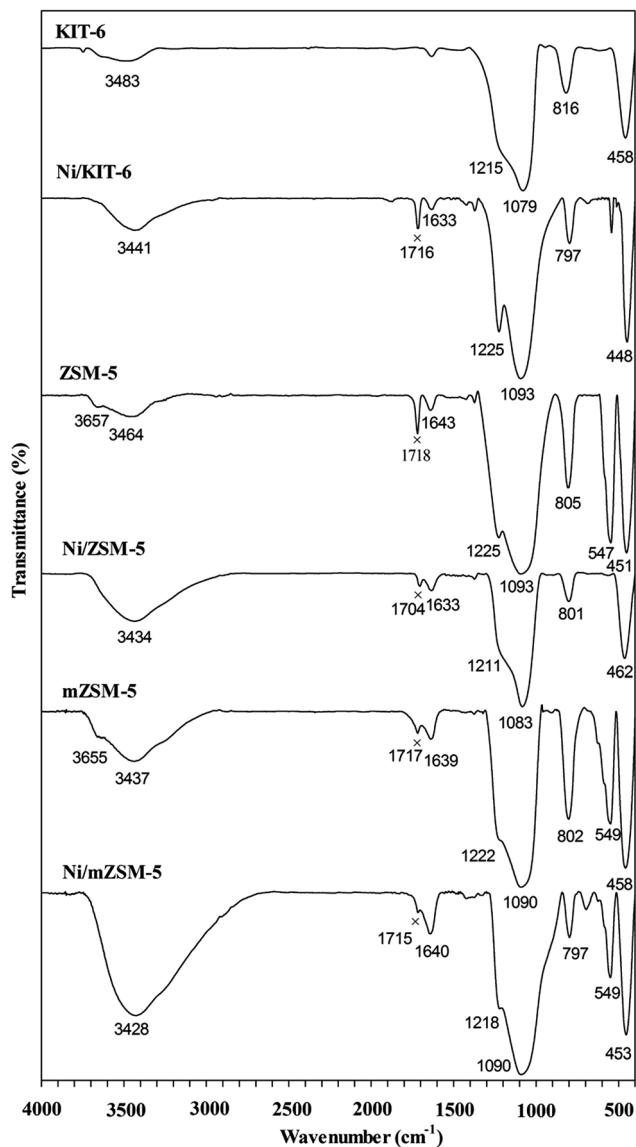


Fig. 8 FT-IR spectra of KIT-6, Ni/KIT-6, ZSM-5, Ni/ZSM-5, mZSM-5 and Ni/mZSM-5. (x Impurity: carbonyl bond of acetone which was used for rinse of the silicon wafer while preparation of KBr pellet).

images). It should be mentioned that after loading Ni nanoparticles on the surface of mZSM-5, the crystalline structure of the zeolite is not destroyed.

The SEM images of the H-mZSM-5 and Ni/H-mZSM-5 are given in Fig. 10. As shown, cubic crystalline structure of H-mZSM-5 and mZSM-5 are the same and the morphology and crystalline structure of H-mZSM-5 are still maintained, which indicates that the structure of mZSM-5 is not changed after acidification (Fig. 10a).

Also, after the deposition of nickel nanoparticles on the surface of the H-mZSM-5, the structure of zeolite is still retained. Moreover, distribution of Ni nanoparticles on the outer surface of the zeolite can be noticed (Fig. 10b-d).

Fig. 11a shows the DRS-UV of mZSM-5, Ni²⁺/mZSM-5 and Fig. 11b shows the DRS-UV of Ni/mZSM-5 and Ni/H-mZSM-5. DRS-UV of Ni²⁺/mZSM-5 is added in order to demonstrate the

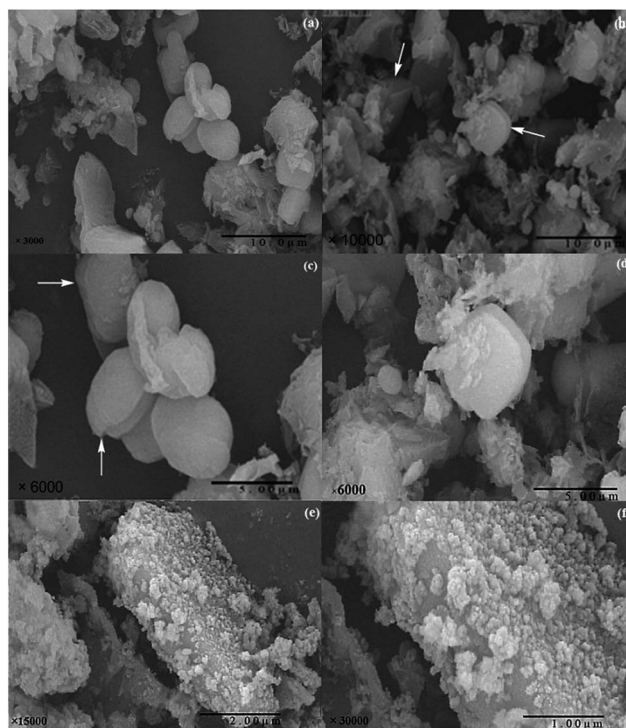


Fig. 9 Scanning electron microscopy (SEM) photographs of (a-d) mZSM-5 and (e and f) Ni/mZSM-5.

difference between DRS-UV of Ni²⁺/mZSM-5 and Ni/mZSM-5. There is no characteristic peak in mZSM-5. In the case of Ni²⁺/mZSM-5, there are no LMCT transitions at wavelengths longer than 250 nm; so, the peaks involve in this case are d-d transitions only (Fig. 11a). Assuming octahedral coordination of Ni(II), the observed absorption bands can be attributed to the electronic transitions of ³T_{1g}(P) ← ³A_{2g}(F) (368 nm) and ³T_{1g}(F) ← ³A_{2g}(F) (576 nm) (Fig. 11a).^{12,51} As shown in Fig. 11b, the DRS-UV of Ni/mZSM-5 and Ni/H-mZSM-5 show feature bands around 205 nm and 330 nm, which are attributed to the presence of Ni

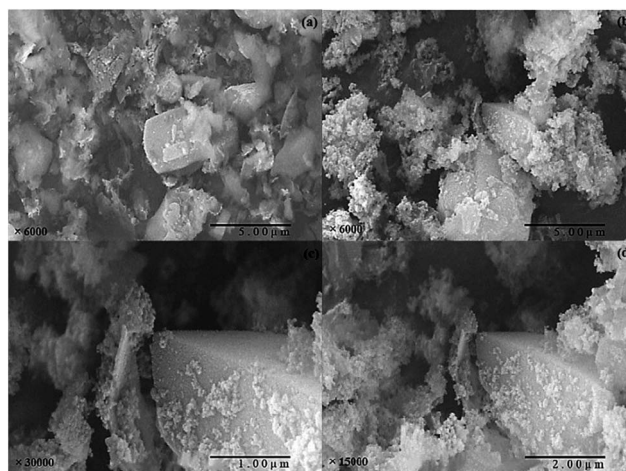


Fig. 10 Scanning electron microscopy (SEM) photographs of (a) H-mZSM-5 and (b-d) Ni/H-mZSM-5.

nanoparticles in these samples.⁵¹ By comparing the two spectra (Fig. 11a and b), it can be found that all peaks of Ni²⁺ disappeared as the result of the reduction of Ni²⁺ to Ni⁰.

Fig. 12a–c shows the TEM images of mZSM-5 and Ni/mZSM-5. The ordered mesostructure of mZSM-5 and the distribution of the Ni nanoparticles in the Ni/mZSM-5 can be seen from Fig. 12a–c. The places with darker contrasts can be correlated to the presence of Ni nanoparticles with different dispersions (Fig. 12c). The small dark spots in the images can be related to Ni nanoparticles with average diameter of ~3–5 nm, and are probably located into the support channels (Fig. 12c(a)). The larger dark areas over the channels most likely correspond to Ni nanoparticle agglomerates on the external surface with an average diameter of ~5–10 nm (Fig. 12c(b)). As can be seen, after the incorporation of Ni nanoparticles in mZSM-5, the mesopore structure still remains (Fig. 12c).

Also, Fig. 12d and e show the TEM images of hierarchical H-mZSM-5 and Ni/H-mZSM-5 zeolites. TEM image of H-mZSM-5 shows that the ordered mesostructure of mZSM-5 is retained (Fig. 12d). However, TEM image of H-mZSM-5 (Fig. 12d) shows some degrees of roughening, which cannot be seen in that of mZSM-5 (Fig. 12a). This result is in accordance with the one

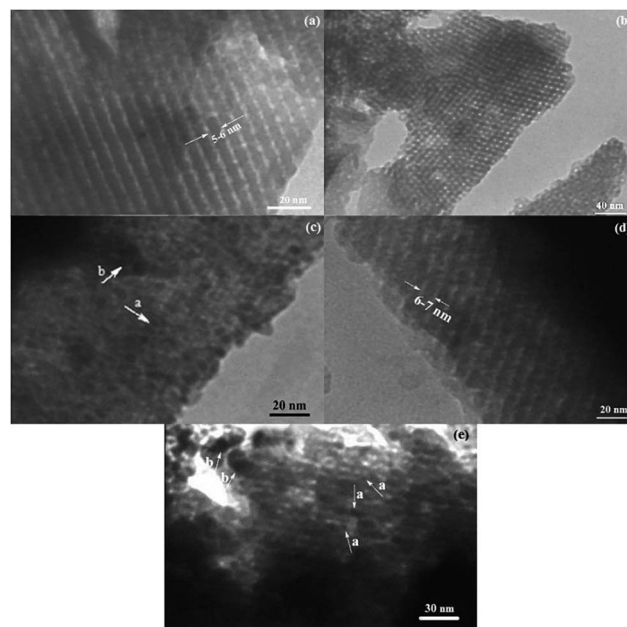


Fig. 12 Transmission electron microscopy (TEM) of (a,b) mZSM-5, (c) Ni/mZSM-5, (d) H-mZSM-5 and (e) Ni/H-mZSM-5.

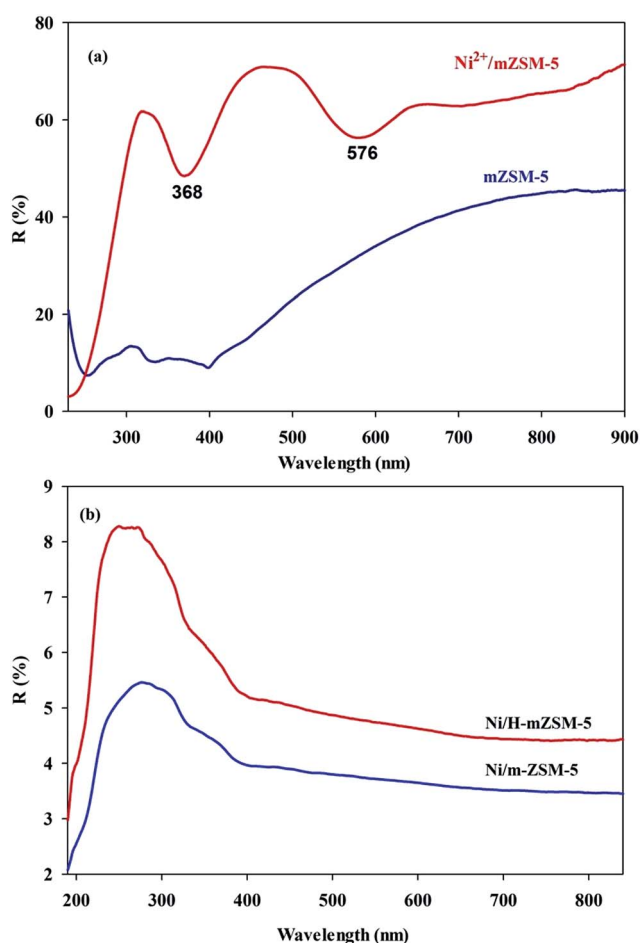


Fig. 11 DRS-UV spectra of (a) mZSM-5 and Ni²⁺/mZSM-5 and (b) Ni/mZSM-5 and Ni/H-mZSM-5.

obtained from pore size distribution curves of mZSM-5 and H-mZSM-5. This roughening places more Ni nanoparticles in the pores of H-mZSM-5 (the Ni contents of the catalysts are presented in Table 2). The small dark spots in the image can be related to Ni nanoparticles in Ni/H-mZSM-5 with various distributions inside and outside the pores (Fig. 12e).

Fig. 13a shows the XPS spectrum of nanoparticles Ni/mZSM-5 obtained from the reduction of nickel(II) chloride hexahydrate by sodium borohydride in the presence of hierarchical zeolite after refluxing for 5 h in water solution at 353 K. The XPS result of Ni nanoparticles dispersed in mZSM-5 media for Ni2p spectrum with the binding energies of Ni2p_{3/2} and Ni2p_{1/2} lying at about 852.7 and 870.4 eV, respectively (see Fig. 13a), meaning that Ni nanoparticles are stable in metallic state in mZSM-5.^{14,52} However, in comparison to the standard binding energy (Ni⁰ with Ni2p_{3/2} of about 852.3 eV and Ni2p_{1/2} of about 869.7 eV),^{14,52} it can be concluded that the Ni peaks in Ni/mZSM-5 slightly shifted to higher binding energy than Ni⁰ standard binding energy. As we know, the position of Ni2p peak is usually influenced by the local chemical/physical environment around Ni species besides the formal oxidation state, and shifts to higher binding energy when the charge density around it decreases.⁵² Therefore, the existence of the acidic sites of the zeolite (with the electron withdrawing nature) around the Ni⁰ species leads to a decrease in the charge density around Ni⁰ and a slight increase in binding energy.²¹

The full XPS spectrum of Ni/mZSM-5 showed peaks of silicon, aluminum, carbon, oxygen and nickel. Carbon peaks correspond to the remaining organic template of TPAOH and P123 (Fig. 13b).

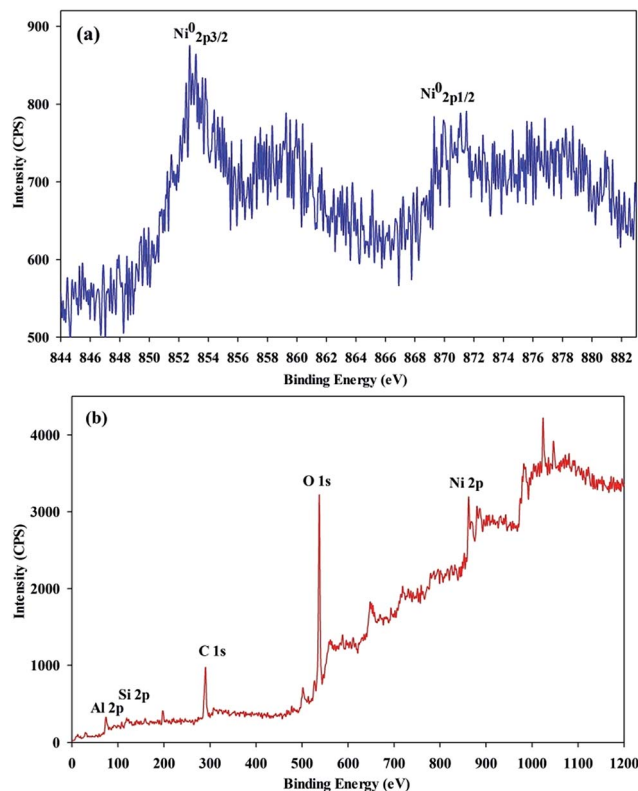


Fig. 13 (a) XPS spectrum of Ni2p of Ni/mZSM-5, (b) full XPS spectrum of Ni/mZSM-5.

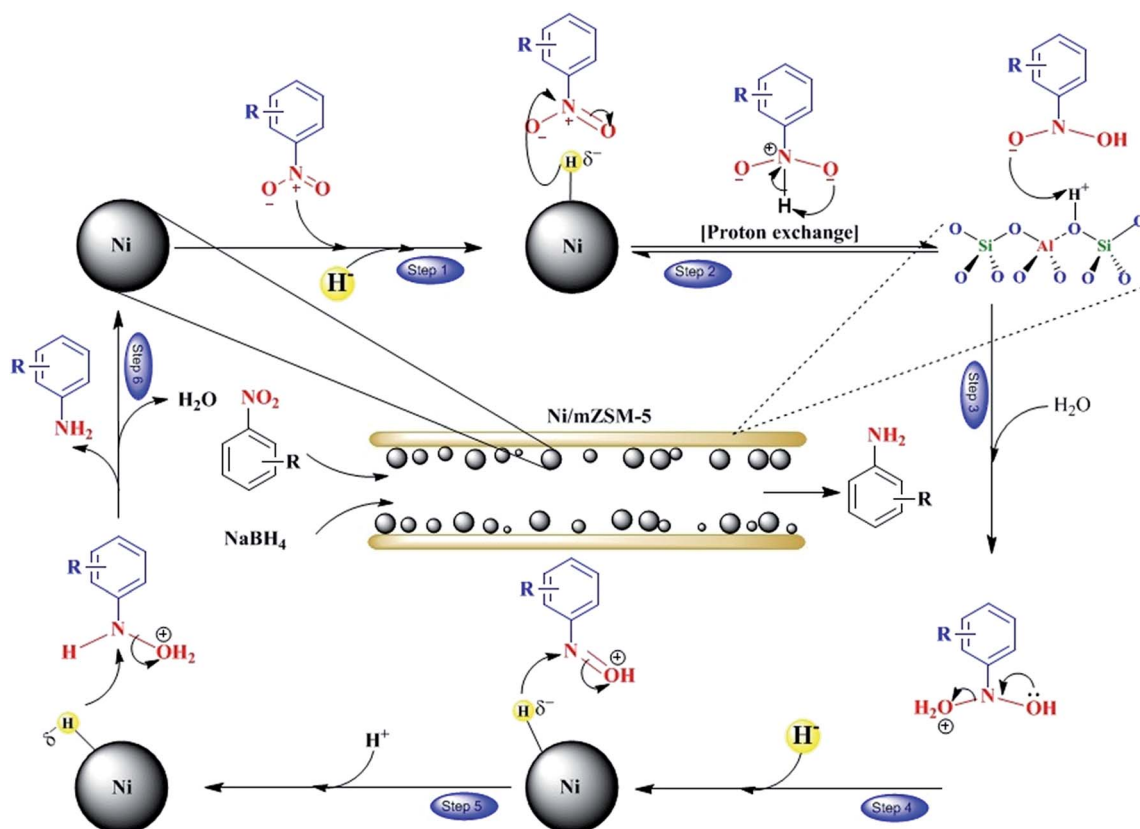
Catalytic activity

The novel hierarchical zeolites containing nickel nanoparticles were synthesized and fully characterized using different methods. The main goal of this catalytic synthesis was to expand the use of these types of zeolites for organic reactions and to investigate the effect of acidic properties of the bifunctional catalyst in the reduction reaction.

Table 2 Effect of $\text{NiCl}_2 \cdot 6\text{H}_2\text{O}$ molar ratio on the catalytic activity^a

Entry	$\text{NiCl}_2 \cdot 6\text{H}_2\text{O}$ (mmol)	Ni content of catalyst (mmol in 0.1 g Ni/mZSM-5)	Reaction time (min)	Yield (%)
1	0.2	0.0907	2	40 ^b
			12	97 ^c
2	0.5	0.2117	2	98 ^c
			15	30 ^b
3	0.7	0.2704	2	98 ^c
			15	20 ^b
4	1	0.3118	2	86 ^d
			15	20 ^b
5	1.2	0.3280	2	20 ^b
			15	81 ^d

^a Reaction conditions: nitrobenzene (2 mmol), Ni/mZSM-5 (0.1 g), H_2O (3 mL), NaBH_4 (8 mmol), room temperature. ^b Monitoring by TLC. ^c Isolated yield after work-up. ^d Isolated yield after column chromatography.



Scheme 1 Possible mechanism of nitrobenzene reduction over Ni/mZSM-5.

The reduction of nitro benzene was chosen as a model reaction to test the catalytic activity of the Ni/mZSM-5 for the reduction of nitro aromatic compounds. This reduction reaction was carried out in water as a green solvent and in room temperature.

To identify the effect of nickel nanoparticles concentration on the reduction reaction, different amounts of $\text{NiCl}_2 \cdot 6\text{H}_2\text{O}$ were examined. The amount of $\text{NiCl}_2 \cdot 6\text{H}_2\text{O}$ to prepare Ni/mZSM-5 was changed from 0 mmol to 1.2 mmol while the other values were constant (the molar ratio of NiCl_2 to NaBH_4 was 1 : 6). Ni contents of the catalysts were determined by Atomic Absorption method and are presented in Table 2. As shown in Table 2, the catalytic activity was improved by increasing the amount of $\text{NiCl}_2 \cdot 6\text{H}_2\text{O}$ from 0.2 to 0.5 mmol. As the catalytic reaction mechanism involves Ni nanoparticle mediated electron transfer from BH_4^- ion to the nitro compounds, the amount of H⁻ sites on the catalyst surface are increased by increasing nickel nanoparticles, and a larger amount of hydride can be transferred to the nitro compounds through the catalyst or a larger amount of H₂ gas can be produced in reduction of nitro compounds.^{12,20,53} Therefore, the catalyst prepared by 0.5 mmol $\text{NiCl}_2 \cdot 6\text{H}_2\text{O}$ showed the best catalytic activity. However, by further increasing the amount of $\text{NiCl}_2 \cdot 6\text{H}_2\text{O}$ (more than 0.5 mmol), the catalytic activity was reduced, which can be explained with the following reasons: After a certain amount of nickel chloride increases, a larger amount of NPs is loaded on the surface of the zeolite that may have caused the hierarchical zeolite pores to narrow. Actually, by increasing the amount of NiCl_2 , the nanoparticle size will increase,^{54,55} the pore size will narrow in some places and it can reduce the rate of reactants diffusion through the pores. Therefore, lower activity of the catalyst prepared with higher NiCl_2 concentration will be expected. However, it doesn't mean that the pores are entirely clogged. Moreover, by increasing the amount of nickel nanoparticles on the surface of the zeolite, Bronsted and Lewis acid sites of the zeolite can be more occupied (Scheme 1). Therefore, as the acidic content of catalyst is reduced, the catalytic activity of the catalyst is reduced as well. It should be noted that the results of this factor represent the dual properties of the acid-metal of the catalyst.

As shown in Table 2, by increasing the amount of $\text{NiCl}_2 \cdot 6\text{H}_2\text{O}$ added to the catalyst, the amount of nickel nanoparticles precipitated on the catalyst surface increases (according to the XPS and DRS UV-Vis results it can be stated that there is just Ni nanoparticles on the surface of the catalyst and there are not any other species of Ni).^{12,14,51,52} However, with a closer look, it can be realized that at higher concentrations of nickel chloride added, the amount of nickel located on the catalyst surface increases to a lesser extent (entry 4 and 5). This could be due to the gradual filling of the hierarchical zeolite pores, which is a good reason for the lower yield and higher reaction time.

To identify the effect of NaBH_4 amount on the conversion of Ni^{2+} to nickel nanoparticle, the Ni/mZSM-5 catalyst was prepared using various amounts of NaBH_4 . Therefore, the amount of $\text{NiCl}_2 \cdot 6\text{H}_2\text{O}$ for the preparation of Ni/mZSM-5 was kept constant (0.5 mmol) and the amount of NaBH_4 added was changed from 1 mmol to 4 mmol, keeping other parameters

Table 3 Effect of NaBH_4 amounts on the synthesis of Ni/mZSM-5^a

Entry	Amount of NaBH_4 (mmol)	Ni content of catalyst (mmol in 0.1 g Ni/mZSM-5)	Reaction time (min)	Yield ^b (%)
1	1	0.1546	2 28	30 ^c 97
2	2	0.1929	2 14	55 ^c 97
3	3	0.2117	2	98
4	4	0.2228	2	98

^a Reaction conditions: nitrobenzene (2 mmol), Ni/mZSM-5 (0.1 g), H₂O (3 mL), NaBH_4 (8 mmol), room temperature. ^b Isolated yield after work-up. ^c Monitoring by TLC.

constant. Ni contents of the catalysts were determined by atomic absorption method and are presented in Table 3. As shown in Table 3, the nickel nanoparticle amount of the catalyst was improved by increasing the amount of NaBH_4 from 1 to 4 mmol. However, the catalyst prepared using 3 mmol NaBH_4 (entry 3) showed the same activity to the catalyst prepared using 4 mmol NaBH_4 (entry 4). According to the results, the amount of 3 mmol of NaBH_4 was chosen to be the optimized amount for the preparation of the catalyst.

The effect of NaBH_4 amount (as a hydride donor) on the reduction of nitrobenzene was investigated in the presence of Ni/mZSM-5 and Ni/H-mZSM-5 as catalysts. The results showed that the yield was increased by increasing the amount of NaBH_4 (until 6 mmol) (Table 4).

With further increase in the NaBH_4 amount, the yield of the reaction remained the same. Therefore, 6 mmol NaBH_4 was the best value because fewer values were not enough for the reduction of the mentioned amount of aromatic nitro compounds and the excess values didn't have any effect on the reaction.

The variations of catalytic activity with various amounts of catalysts were studied (Table 5). In general, there was an upward trend of aniline yield by raising the catalyst amounts. According to the results, 0.04 g and 0.02 g were the best values for Ni/mZSM-5 and Ni/H-mZSM-5, respectively, and the

Table 4 Effect of reducing agent on the nitrobenzene reduction^a

Entry	Amount of NaBH_4 (mmol)	Ni/H-mZSM-5 (0.04 g)		Ni/mZSM-5 (0.1 g)	
		Reaction time (min)	Yield ^b (%)	Reaction time (min)	Yield ^b (%)
1	2	2 25	25 ^c 86 ^d	—	—
2	4	2 8	40 ^c 98	2 11	50 ^c 98
3	6	2	97	2	97
4	8	2	97	2	97

^a Reaction conditions: nitrobenzene (2 mmol), H₂O (3 mL), room temperature, catalyst (Ni/H-mZSM-5 or Ni/mZSM-5). ^b Isolated yield after work-up. ^c Monitoring by TLC. ^d Isolated yield after column chromatography.

Table 5 Effect of catalyst amount on the nitrobenzene reduction^a

Entry	Ni/mZSM-5			Ni/H-mZSM-5		
	Amount of catalyst (g)	Reaction time (min)	Yield ^b (%)	Amount of catalyst (g)	Reaction time (min)	Yield ^b (%)
1	0.02	8	96	0.01	2	35 ^c
2	0.03	5	95	0.02	10	95
				0.02	2	97
3	0.04	2	97	0.03	2	95
4	0.06	2	97	0.04	2	97
5	0.08	2	96	—	—	—
6	0.10	2	97	—	—	—

^a Reaction conditions: nitrobenzene (2 mmol), H₂O (3 mL), NaBH₄ (6 mmol), room temperature. ^b Isolated yield after work-up. ^c Monitoring by TLC.

additional amounts of catalysts did not have any effect on the catalytic activity. It should be noted that using low amounts of catalysts and NaBH₄ in this reaction shows excellent catalytic activity of these catalysts. Moreover, the catalytic activity of Ni/H-mZSM-5 is relatively higher than that of Ni/mZSM-5, which may be related to the higher acidic content of Ni/H-mZSM-5 (according to the proposed mechanism presented in Scheme 1).

Another important issue concerning the application of a heterogeneous catalyst is reusability and stability under reaction conditions. To gain insight into this issue, catalyst recycling experiments were carried out using a reduction reaction over Ni/mZSM-5 and Ni/H-mZSM-5. The results are shown in Table 6. After each cycle, the catalyst was filtered off, washed with water (10 mL) and ethanol (3 mL × 5 mL). Then, it was dried in an oven at 60 °C and reused in the reduction reaction. The results showed that both catalysts could be reused 7 times without any modification and no significant loss of activity performance was observed.

It should be mentioned that there was very low Ni leaching (about 1%) during the reaction and the catalysts exhibited high stability even after 7 cycles (Table 6). Also, the acidic

Table 6 The catalysts reusability for the nitrobenzene reduction

Cycle	Ni content of catalyst (mmol in 0.04 g Ni/mZSM-5) ^a		Ni content of catalyst (mmol in 0.02 g Ni/H-mZSM-5) ^b	
	Yield ^c (%)	Yield ^c (%)	Yield ^c (%)	Yield ^c (%)
Fresh	0.0847	97	0.0464	97
1	0.0844	95	0.0463	96
2	0.0843	94	0.0462	93
3	0.0841	94	0.0461	93
4	0.0840	91	0.0461	92
5	0.0838	91	0.0460	92
6	0.0837	90	0.0459	91

^a Reaction conditions: nitrobenzene (2 mmol), H₂O (3 mL), NaBH₄ (6 mmol), Ni/mZSM-5 (0.04 g), room temperature. ^b Reaction conditions: nitrobenzene (2 mmol), H₂O (3 mL), NaBH₄ (6 mmol), Ni/H-mZSM-5 (0.02 g), room temperature. ^c Isolated yield after work-up.

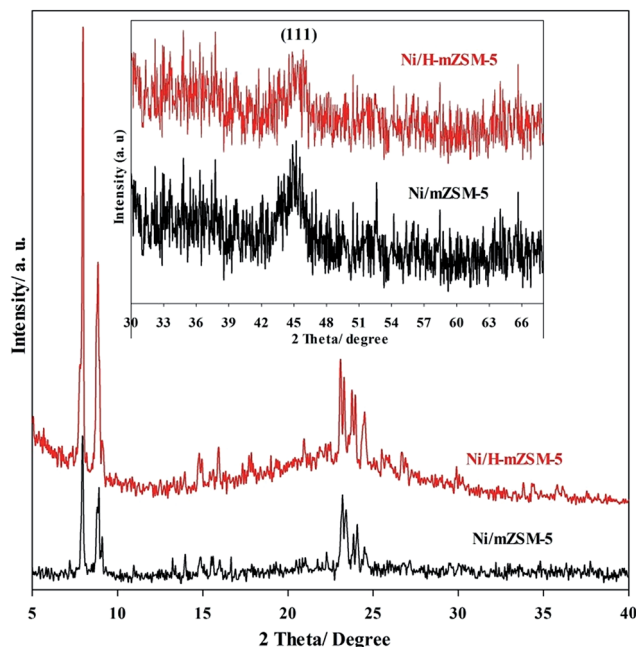


Fig. 14 XRD patterns of the used Ni/mZSM-5 and Ni/H-mZSM-5 catalysts after the fifth run of the recycle reaction and inside: used Ni/mZSM-5 and Ni/H-mZSM-5 after the fifth run of the recycle reaction burned in 400 °C for 4 h ($2\theta = 30-66$).

properties of reused Ni/H-mZSM-5 catalyst (after 5 runs) were investigated by TPD. The results showed that the amount of acidic sites of the catalyst is decreased only about 5% (0.87

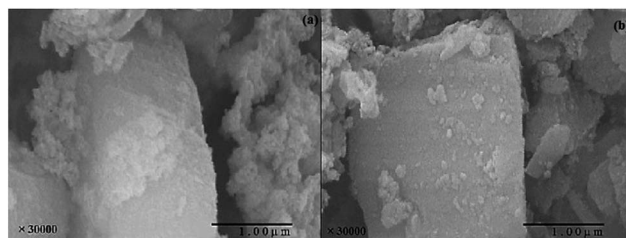


Fig. 15 Scanning electron microscopy (SEM) photographs of the used (a) Ni/mZSM-5 and (b) Ni/H-mZSM-5 catalysts after the fifth run of the recycle reaction.

Table 7 Effect of catalyst for the nitrobenzene reduction^a

Entry	Catalyst	Reaction time (min)	Yield (%)
1	Without catalyst	120	10 ^b
2	ZSM-5	60	15 ^b
3	mZSM-5	60	20 ^b
4	Ni ²⁺ /mZSM-5	60	40 ^b
5	Ni/KIT-6	31	95 ^c
6	Ni/ZSM-5	26	96 ^c
7	Ni/m-ZSM-5	2	97 ^c

^a Reaction conditions: nitrobenzene (2 mmol), H₂O (3 mL), catalyst (0.04 g), NaBH₄ (6 mmol), room temperature. ^b Isolated yield after column chromatography. ^c Isolated yield after work-up.

Table 8 Reduction of various nitro aromatic compounds over Ni/mZSM-5^a

0.04 g of Ni/mZSM-5
6 mmol NaBH₄
r.t., 3 ml H₂O

Entry	Substrate	Product	Yield ^b (%)	Time (min)	TON/TOF (min ⁻¹)	Mp (°C)	
						Found	Reported (ref.)
1			97	2	22.9/11.5	—	—
2			96	1	22.7/22.7	171–173	174 (ref. 11)
3			95	3	22.4/7.5	121–123	123 (ref. 11)
4			96	2	22.7/11.3	185–189	187 (ref. 15)
5			91 ^c	12	21.5/1.8	47–50	50 (ref. 11)
6			92 ^{c,d}	16	10.9/0.7	62–65	66 [CRC book]
7			95	3	22.4/7.5	69–71	71 (ref. 11)
8			96	2	22.7/11.3	121–123	122 (ref. 11)
9			95	20	22.4/1.1	119–122	120 (ref. 11)

Table 8 (Contd.)

Entry	Substrate	Product	Yield ^b (%)	Time (min)	TON/TOF (min ⁻¹)	Mp (°C)	
						Found	Reported (ref.)
10			89 ^c	60	21.0/0.4	51–56	55 [CRC book]
11			94	2	22.2/11.1	59–62	63 [CRC book]
12			95	2	22.4/11.2	88–91	90 [CRC book]
13			96	3	22.7/7.6	61–63	63 [CRC book]
14			96	3	22.7/7.6	140–143	141 (ref. 11)
15			95 ^d	4	11.2/2.8	100–104	102 (ref. 11)
16			90 ^c	25	21.3/0.9	—	—
17			92 ^{c,d}	45	10.9/0.2	98–99	99 [CRC book]

Table 8 (Contd.)

Entry	Substrate	Product	Yield ^b (%)	Time (min)	TON/TOF (min ⁻¹)	Mp (°C)	
						Found	Reported (ref.)
18			84 ^c	65	19.8/0.3	—	—
19			96 ^e	5	22.7/4.6	—	—

^a Reaction conditions: nitro aromatic compound (2 mmol), Ni/mZSM-5 (0.04 g), NaBH₄ (6 mmol), H₂O (3 mL), room temperature. ^b Isolated yield after work-up. ^c Isolated yield after column chromatography. ^d Substrate (1 mmol). ^e Scale-up condition: nitrobenzene (50 mmol), catalyst (1 g), NaBH₄ (150 mmol), H₂O (200 mL), room temperature.

mmol g⁻¹). However, it had no significant effect on the catalytic activity as it can be seen from Table 6.

In addition, the XRD patterns of the used catalysts after five runs showed that the structure of the catalysts is well retained (Fig. 14).

Also, SEM images of the catalysts (Ni/mZSM-5 and Ni/H-mZSM-5) recovered from the fifth run of the recycle reaction are presented in Fig. 15. Comparison of these images with SEM images of the fresh catalysts (Fig. 9 and 10) indicates that the structure of the zeolites is well retained even after the fifth run of the recycle reaction. Therefore, the catalysts exhibit high stability over 5 recycles, which is very important for the catalyst applications.

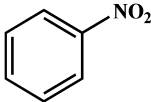
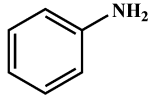
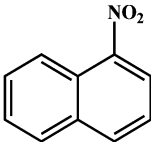
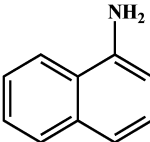
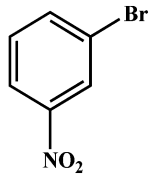
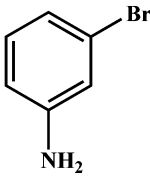
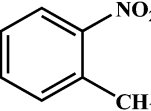
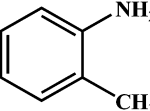
The catalytic activity of the Ni/mZSM-5 in the reduction of nitrobenzene was compared with mZSM-5, Ni/ZSM-5, Ni/KIT-6 and Ni²⁺/mZSM-5. The results are given in Table 7. The result highlights the important role of the catalyst in this reaction. As can be seen, the reaction performance without catalyst will be only 10% (entry 1). It is noteworthy to say that NaBH₄ is considered a mild hydride donor agent, which is not a good reagent for reducing the nitro groups. By using ZSM-5 and mZSM-5 catalysts (entries 2 and 3), the yield was increased slightly because the acid sites of the zeolites cause nitro groups to activate. Using Ni²⁺/mZSM-5 (entry 4), the yield of nitro benzene reduction was increased to 40% due to the role of Ni ions as species to transfer hydride ions from NaBH₄ to nitro groups.

Comparing the activity of Ni/ZSM-5, Ni/KIT-6 and Ni/mZSM-5, the latter showed the best performance (entries 5–7). Actually, according to the mechanism presented in Scheme 1, the reductions of nitro groups need acid sites to go faster. In this regard, Ni/ZSM-5 and Ni/m-ZSM-5 showed a higher activity due to having more acidic sites than those of Ni/KIT-6. Moreover, Ni/mZSM-5 showed higher performance than Ni/ZSM-5, which is related to the hierarchical structure of mZSM-5. The hierarchical structure containing microporous and mesoporous buildings cause easier access of reactants to the active sites of the catalyst.

In further studies, reduction reactions of different nitro aromatic compounds were carried out over the Ni/mZSM-5 as catalyst after ascertaining the optimum experimental conditions. These reactions were performed in the aqueous media and at room temperature. The results are shown in Table 8. In all cases, the reduction reactions proceed rapidly to give the corresponding aniline derivatives in excellent yield/selectivity and short reaction times. The turn-over frequency (TOF) and turn-over number (TON) values indicate that Ni/mZSM-5 is a very active catalyst for this kind of reaction. TOF and TON being defined as the (mol product/(mol catalyst. min)) and (mol product/(mol catalyst)), respectively, and these were calculated from the isolated yield, the amount of nickel used and the reaction time.

This reduction system was easily scaled-up and served for the synthesis of aniline at several gram scales. The reduction of

Table 9 Reduction of various aromatic nitro compounds over Ni/H-mZSM-5^a

Entry	Substrate	Product	Yield ^b (%)	Time (min)	TON/TOF (min ⁻¹)	Mp (°C)	
						Found	Reported (ref.)
1			97 ^c	2	20.9/10.5	—	—
			97 ^d	3	41.8/13.9		
2			97 ^c	3	20.9/7.0	47–50	50 (ref. 11)
			96 ^d	15	41.4/2.8		
3			97 ^c	15	20.9/1.4	119–122	120 (ref. 11)
			98 ^d	20	42.2/2.1		
4			92 ^{c,e}	20	19.8/1.0	—	—
			91 ^{d,e}	30	39.2/1.3		

^a Reaction conditions: nitro aromatic compound (2 mmol), NaBH₄ (6 mmol), H₂O (3 mL), room temperature. ^b Isolated yield after work-up. ^c Ni/H-mZSM-5 (0.04 g). ^d Ni/H-mZSM-5 (0.02 g). ^e Isolated yield after column chromatography.

nitrobenzene into aniline was performed on a 25-time scale-up (Table 8, entry 19), representing the high activity of the catalyst.

Also, to compare the activity of Ni/mZSM-5 and Ni/H-mZSM-5, the reduction reaction of some nitro compounds was observed on Ni/H-mZSM-5 (Table 9). As can be seen, compared to Ni/mZSM-5, Ni/H-mZSM-5 depicts a shorter reaction time, and lower amounts of catalyst in the reduction reaction. The TOF value indicates that Ni/H-mZSM-5 is a more active catalyst for this kind of reaction. It may be related to more acidic properties of the Ni/H-mZSM-5 compared to Ni/mZSM-5 (according to the mechanism presented in Scheme 1).

In order to prove the heterogeneous nature of the catalysts and the absence of Ni leaching, heterogeneity tests were performed for the optimized reduction reaction of 3-bromonitrobenzene, in which the catalysts (Ni/mZSM-5 and Ni/H-mZSM-5) were separated from the reaction mixture at approximately 50% conversion of the starting material through centrifugation. The reaction progress in the filtrate was monitored. No further reducing reaction occurred even at extended times, indicating that the nature of the reaction process is heterogeneous and there is not any progress for the reaction in the homogeneous phase (it should be mentioned that reduction of 3-bromonitrobenzene was preferred to investigate the heterogeneity test instead of nitrobenzene, because of the short time span nitrobenzene takes for reduction (2–3 min), the time is not enough to investigate the heterogeneity of the catalysts).

Intermediates and reaction mechanism

Two probable pathways (either the direct route or the condensation route) are described as mechanistic issues of the reduction of nitro group to amino group by Corma, *et al.*⁵⁶ In the direct route, the nitro compound can reduce to a nitroso compound, which further proceeds to provide the hydroxylamine, finally giving rise to amine. In the condensation route, the initially formed nitroso compound may condense with hydroxylamine to produce the azoxy compound, which then may undergo further reduction to azo, hydrazo, and finally the amine compound.⁵⁷ To find out the exact pathway with the catalytic system Ni/mZSM-5, we carried out our reduction reaction of nitrobenzene with the intermediate compounds. When we used hydrazobenzene and azobenzene instead of nitrobenzene, and kept the same experimental conditions, we obtained the amine product detected by GC with only 13% and 17% after 20 and 30 minutes, respectively. In contrast, when we used nitroso benzene and phenylhydroxylamine, the reactions were very fast and we obtained 98% and 99% of the amine product in only one minute.

It is wise to mention that the produced hydroxylamine is relatively difficult to reduce further because the N–O bond is strengthened by electron-withdrawing groups. Therefore, the rate of reduction of hydroxylamine to amine is slower than that of formation of hydroxylamine, which permits its isolation over a period of time.⁵⁸ Hence, in order to see the intermediates of nitrosobenzene and phenylhydroxylamine, the reduction reaction of 2,4-dimethyl nitrobenzene, which takes a long time, was studied. TLC and HPLC studies did not show any traces of

unreacted nitrosobenzene and phenylhydroxylamine. The absence of nitrosobenzene and phenylhydroxylamine in the reaction mixture signifies that they get very strongly adsorbed onto the catalyst surface and react before desorption.⁵⁹ From these results, it is concluded that the condensation route is disfavored over the direct route. Indeed, intermediates of the direct route are completely reduced in a shorter time, and the high rate of reduction of nitrosobenzene and phenylhydroxylamine could also explain the absence of condensation between these two products to give azoxybenzene.

Conclusion

In conclusion, as a hierarchical zeolite, mZSM-5 was successfully synthesized using KIT-6 as a mesoporous silica source, modified with Ni nanoparticles and exhibited good catalytic performance in reduction of nitro aromatic compounds at room temperature in an aqueous media.

N₂ adsorption–desorption isotherms showed that Ni/mZSM-5 has a mesoporous-microporous structure. The existence of the mesopores in the zeolite structure accelerates the molecular transportation and also causes high accessibility of acid sites of the zeolite. These features increase the activity/stability of the catalyst. A comparison between Ni/mZSM-5 and Ni/H-mZSM-5 showed superior activities of Ni/H-mZSM-5 catalyst, which is possibly due to the existence of more acidic sites in the Ni/H-mZSM-5 structure rather than Ni/mZSM-5. Additionally, upon the completion of the reactions, the catalysts could be removed from the reaction medium easily and reused for several cycles without any significant decrease in the catalytic activity/stability. These unique features open new perspectives for the application of these types of hierarchical zeolites in other organic reactions instead of using traditional zeolites.

Notes and references

- 1 D. M. Dotzauer, S. Bhattacharjee, Y. Wen and M. L. Bruening, *Langmuir*, 2009, **25**, 1865.
- 2 D. Cantillo, M. M. Moghaddam and C. O. Kappe, *J. Org. Chem.*, 2013, **78**, 4530.
- 3 G. W. Lamb, F. A. Al-Badran, J. M. J. Williams and S. T. Kolaczowski, *Chem. Eng. Res. Des.*, 2010, **88**, 1533.
- 4 J. Zhou, J. Dai, G. Q. Bian and C. Y. Li, *Coord. Chem. Rev.*, 2009, **253**, 1221.
- 5 R. Shen and S. A. Andrews, *Water Res.*, 2013, **47**, 2446.
- 6 A. Kumar, D. Nepak and D. Srinivas, *Catal. Commun.*, 2013, **37**, 36.
- 7 X. F. Wu, A. Petrosyan, T. V. Ghochikyan, A. S. Saghyan and P. Langer, *Tetrahedron Lett.*, 2013, **54**, 3158.
- 8 F. C. Lizana, S. G. Quero and M. A. Keane, *Catal. Commun.*, 2008, **9**, 475.
- 9 A. Saha and B. Ranu, *J. Org. Chem.*, 2008, **73**, 6867.
- 10 S. Farhadi and F. Siadatnasab, *J. Mol. Catal. A: Chem.*, 2011, **339**, 108.
- 11 S. Gowda, B. K. K. Gowda and D. C. Gowda, *Synth. Commun.*, 2003, **33**, 281.
- 12 R. J. Kalbasi, A. A. Nourbakhsh and F. Babaknezhad, *Catal. Commun.*, 2011, **12**, 955.
- 13 J. N. Solanki and Z. V. P. Murthy, *Ind. Eng. Chem. Res.*, 2011, **50**, 7338.
- 14 H. Wena, K. Yao, Y. Zhang, Z. Zhou and A. Kirschning, *Catal. Commun.*, 2009, **19**, 1207.
- 15 J. F. Quinn, C. E. Bryant, K. C. Golden and B. T. Gregg, *Tetrahedron Lett.*, 2010, **51**, 786.
- 16 R. J. Rahaim, J. Robert and E. Maleczka, *Org. Lett.*, 2005, **7**, 5087.
- 17 P. Veerakumara, M. Velayudhamb, K. L. Lub and S. Rajagopala, *Appl. Catal., A*, 2012, **439–440**, 197.
- 18 A. Rajapakse and K. S. Gates, *J. Org. Chem.*, 2012, **77**, 3531.
- 19 M. B. Gawande, H. Guo, A. K. Rathi, P. S. Branco, Y. Chen, R. S. Varmad and D. L. Peng, *RSC Adv.*, 2013, **3**, 1050.
- 20 M. A. Harrad, B. Boualy, L. El Firdoussi, A. Mehdi, C. Santi, S. Giovagnoli, M. Nocchetti and M. A. Ali, *Catal. Commun.*, 2013, **32**, 92.
- 21 R. J. Kalbasi, N. Mosaddegh and A. Abbaspourrad, *Appl. Catal., A*, 2012, **423–424**, 78.
- 22 R. J. Kalbasi, N. Mosaddegh and A. Abbaspourrad, *Tetrahedron Lett.*, 2012, **53**, 3763.
- 23 D. Shah and H. Kaur, *J. Mol. Catal. A: Chem.*, 2014, **381**, 70.
- 24 M. Jacquin, D. J. Jones, J. Roziere, S. Albertazzi, A. Vaccari, M. Lenarda, L. Storaro and R. Ganzerla, *Appl. Catal., A*, 2003, **251**, 131.
- 25 A. Hakki, R. Dillert and D. W. Bahnemann, *ACS Catal.*, 2013, **3**, 565.
- 26 R. J. Kalbasi, A. R. Massah and A. Shafiei, *J. Mol. Catal. A: Chem.*, 2011, **335**, 51.
- 27 F. Ocampo, J. A. Cunhab, M. R. de Lima Santosb, J. P. Tessonierc, M. M. Pereirab and B. Louis, *Appl. Catal., A*, 2010, **390**, 102.
- 28 Y. Tao, H. Kanoh and K. Kaneko, *J. Am. Chem. Soc.*, 2003, **125**, 6044.
- 29 K. Na, M. Choi and R. Ryoo, *Microporous Mesoporous Mater.*, 2013, **166**, 3.
- 30 K. Egeblad, C. H. Christensen, M. Kustova and C. H. Christensen, *Chem. Mater.*, 2008, **20**, 946.
- 31 J. C. Groen, T. Bach, U. Ziese, A. M. Paulaime-van Donk, K. P. de Jong, J. A. Moulijn and J. Pérez-Ramírez, *J. Am. Chem. Soc.*, 2005, **127**, 10792.
- 32 R. Chal, R. Cacciaguerra, S. van Donk and C. Ge-radin, *Chem. Commun.*, 2010, **46**, 7840.
- 33 K. Na and G. A. Somorjai, *Catal. Lett.*, 2015, **145**, 193.
- 34 J. Perez-Ramirez, C. H. Christensen, K. Egeblad, C. H. Christensen and J. C. Groen, *Chem. Soc. Rev.*, 2008, **37**, 2530.
- 35 S. L. Orozco, A. Inayat, A. Schwab, T. Selvam and W. Schwieger, *Adv. Mater.*, 2011, **23**, 2602.
- 36 J. Zheng, X. Zhang, Y. Zhang, J. Maa and R. Li, *Microporous Mesoporous Mater.*, 2009, **122**, 264.
- 37 M. S. Holm, E. Taarning, K. Egeblad and C. H. Christensen, *Catal. Today*, 2011, **168**, 3.
- 38 D. P. Serrano, R. A. Garcia, G. Vicente, M. Linares, D. Prochazkova and J. Cejka, *J. Catal.*, 2011, **279**, 366.

- 39 R. J. Kalbasi and N. Mosaddegh, *C. R. Chim.*, 2012, **15**, 988.
- 40 N. Chu, J. Yang, C. Li, J. Cui, Q. Zhao, X. Yin, J. Lu and J. Wanga, *Microporous Mesoporous Mater.*, 2009, **118**, 169.
- 41 F. Kleitz, S. H. Choi and R. Ryoo, *Chem. Commun.*, 2003, **17**, 2136.
- 42 A. R. Massah, R. J. Kalbasi and A. Shafiei, *Monatsh. Chem.*, 2012, **143**, 643.
- 43 K. S. W. Sing, *Pure Appl. Chem.*, 1982, **54**, 2201.
- 44 Z. Yang, Y. Xia and R. Mokaya, *Adv. Mater.*, 2004, **16**, 727.
- 45 K. Sadowska, A. Wach, Z. Olejniczak, P. Kustrowski and J. Datka, *Microporous Mesoporous Mater.*, 2013, **167**, 82.
- 46 P. Sazama, B. Wichterlova, J. Dedecek, Z. Tvaruzkova, Z. Musilova, L. Palumbo, S. Sklenak and O. Gonsiorova, *Microporous Mesoporous Mater.*, 2011, **143**, 87.
- 47 C. Feng Song, M. K. Lu, F. Gu, S. W. Liu, S. F. Wang, D. Xu and D. R. Yuan, *Inorg. Chem. Commun.*, 2003, **6**, 523.
- 48 Y. Zheng, K. Ma, H. Wang, X. Sun, J. Jiang, C. Wang, R. Li and J. Ma, *Catal. Lett.*, 2008, **124**, 268.
- 49 N. Y. Topsoe, K. Pedersen and E. G. Derouane, *J. Catal.*, 1981, **70**, 41.
- 50 A. J. J. Koekkoek, H. Xin, Q. Yang, C. Li and E. J. M. Hensen, *Microporous Mesoporous Mater.*, 2011, **145**, 172.
- 51 S. Kim, B. K. Yoo, K. Chun, W. Kang, J. Choo, M. S. Gong and S. W. Joo, *J. Mol. Catal. A: Chem.*, 2005, **226**, 231.
- 52 O. Metin and S. Ozkar, *J. Mol. Catal. A: Chem.*, 2008, **295**, 39.
- 53 R. J. Kalbasi and F. Zamani, *RSC Adv.*, 2014, **4**, 7444.
- 54 Y. Zhai, Y. Dou, X. Liu, S. S. Park, C. S. Ha and D. Zhao, *Carbon*, 2011, **49**, 545.
- 55 S. E. Bozbag, L. C. Zhang, M. Aindow and C. Erkey, *J. Supercrit. Fluids*, 2012, **66**, 265.
- 56 A. Corma, P. Concepción and P. Serna, *Angew. Chem., Int. Ed.*, 2007, **46**, 7266.
- 57 M. Baron, E. Métay, M. Lemaire and F. Popowycz, *Green Chem.*, 2013, **15**, 1006.
- 58 F. Li, J. Cui, X. Qian and R. Zhanga, *Chem. Commun.*, 2004, 2338.
- 59 K. Layek, M. L. Kantam, M. Shirai, D. Nishio-Hamane, T. Sasaki and H. Maheswaran, *Green Chem.*, 2012, **14**, 3164.